# Estimating Crown Defoliation and the Chemical Constituents in Needles of Scots Pine (*Pinus sylvestris* L.) Trees by Laboratory Acquired Hyperspectral Data

**GEDIMINAS MASAITIS*, GINTAUTAS MOZGERIS AND ALGIRDAS AUGUSTAITIS**
*Institute of Forest Management and Wood Science, 'Aleksandras Stulginskis' University, Studentu str. 13, LT-53362, Akademija, Kaunas r. Lithuania, Tel. +370 37 752291, e-mail: gediminas.masaitis@asu.lt*

**Masaitis, G, Mozgeris, G. and Augustaitis, A.** 2014. Estimating Crown Defoliation and the Chemical Constituents in Needles of Scots Pine (*Pinus sylvestris* L.) Trees by Laboratory Acquired Hyperspectral Data. *Baltic Forestry* 20(2): 314 –325.

*Abstract*

The studies, which involve the potential of imaging spectrometry, are among the most promising ones in forest health assessment. This study estimated crown defoliation and the concentrations of some chemical constituents in the needles of Scots pine (*Pinus sylvestris* L.) trees using laboratory acquired hyperspectral data. Needle samples from 67 Scots pine trees, which showed crown defoliation within the range from 0% to 80% (using 5% gradation), were collected in two mature stands located in the eastern Lithuania. The concentrations of ten chemical elements in the needles were also measured. The hyperspectral reflectance data of the needle samples was recorded under laboratory conditions using a VNIR 400H portable hyperspectral imaging camera operating in the 400–1,000 nm range. Principal component analysis and linear discriminant analysis were used to classify the needle samples into defoliation classes and partial least squares regression was used to predict the concentration of chemical constituents by means of hyperspectral reflectance data. Spectral reflectance data was found to poorly discriminate the needle samples into defoliation classes assessed using 5% steps (kappa statistic was 0.29 and 0.26 for the previous and current year needles, respectively). However, combining the samples into four damage classes, according to the UNECE/FAO definition (none: under 10%; slight: > 10–25%; moderate: > 25–60% and severe: over 60%) improved the spectral reflectance data discrimination ability significantly for the previous year (kappa statistic was 0.50), but not significantly for the current year (kappa statistic was 0.35) needles. Classification into three damage classes (under 30%; > 30–50% and over 50%) was perfect (kappa statistic 1.0). A moderate prediction potential was found for the nitrogen (correlation coefficient between actual and predicted values estimated using cross-validation, $R$ = 0.61), phosphorus ($R$ = 0.57), zinc ($R$ = 0.57), calcium ($R$ = 0.56), manganese ($R$ = 0.49) and potassium ($R$ = 0.40) concentrations, but was poor for boron ($R$ = 0.33), iron ($R$ = 0.26), magnesium ($R$ = 0.20) and copper ($R$ = 0.20) in the current year needles.

**Key words:** hyperspectral reflectance, hyperspectral imaging, Scots pine, defoliation, chemical constituents

## Introduction

In Lithuania, forest health has been monitored for more than 25 years (Ozolinčius and Stakėnas 1996). Tree crown defoliation is considered to be one of the key indicators of tree health (Ozolinčius 1999). Assessment of tree crown defoliation in forests represents an early warning system for the response of forest ecosystems to various stress factors (Fischer et al. 2012) and estimation of this parameter is based mainly on field measurements that visually assess the density of tree crowns in forests (Eichhorn et al. 2010). Defoliation assessment, therefore, relies on the experience and skills of the observer and tends to have some level of subjectivity (Ferretti 1998). Furthermore, the method is very time and labour consuming.

Remote sensing is considered to be an operational tool in forest health assessment, already was used for several decades and is discussed in numerous research and technical publications (Ciesla 2000, Solberg et al. 2004, Wulder et al. 2006). The solutions range from satellite imagery based techniques (Ciesla et al. 1989, Hildebrandt 1993, Zawila-Niedzwiecki 1996, Ardö 1998, Heikkilä 2002) to aerial photography applications (Kuhl 1989, Wulder et al. 2006). In Lithuania, some studies attempted to utilize the potential of remote sensing to assess forest health over extensive areas. The possibilities of estimating tree crown defoliation were examined using spectrazonal aerial photography (Daniulis and Mozgeris, 1993) and digital orthophotos based on conventional and small-format aerial photography acquired using ultra-light aircraft (Eigirdas et al. 2013, Mozgeris and Augustaitis 2013). Nevertheless the experience gained from these studies was never practically introduced into forest health monitoring. One of the possible reasons was that remote sensing had never

been found to be superior to visual estimation of tree crown defoliation in the field. It is usually used for conventional forest inventory applications and may be unsuitable for forest health assessment.

The assessment of forest health becomes more comprehensive, when measurements of chemical constituents in the foliage of forest trees is also included (Huber et al. 2008, Moorthy et al. 2008, Wang and Li 2012). Along with chlorophyll content, the assessment of concentrations of macro-elements (nitrogen, potassium and phosphorus) is of special interest because these elements are the most important ones for the growth and development of plants (Kokally and Clark 1999, Asner and Martin 2008, Axelsson et al. 2013). Furthermore, knowing the concentrations of micro-elements (calcium, magnium, zinc, boron, copper, manganese, and iron) could expand our knowledge about the relationship between the foliage chemical constituents and the condition of forest trees. However, acquiring such information, based on laboratory chemical analyses, is time consuming and expensive, thus making them hard to apply in extensive forest health monitoring projects.

However, along with the progress in technology, forestry continually gains new and modern solutions that allow us to obtain information that cannot be observed by the naked eye and to reduce the amount of time-consuming field or laboratory work. The hyperspectral imaging systems were invented relatively recently, in the late 1970s (Goetz et al. 1985), and can sense very subtle differences in the intensity of electromagnetic radiation. Hyperspectral sensing has become recognised as the most advanced remote sensing technique for collecting and processing reflectance data from electromagnetic radiation (Im and Jensen 2008, Eismann 2012).

Hyperspectral imaging systems acquire images of an object in many narrow (nanometre level) contiguous spectral bands. Depending on the construction, they can sense reflected or emitted electromagnetic radiation in a range stretching from ultraviolet (from 200 nm) to thermal (up to 15,000 nm) waves (Im and Jensen 2008). These instruments can collect hundreds of spectral bands for every pixel of an image. The result is a 'package' of images, in which pixels of each image are recorded in a single spectral band, i.e. the amount of images in this 'package' is equal to the number of acquired spectral bands. Such 'packages' are called hyperspectral cubes. The XY axis of a cube represents spatial data and the Z axis represents spectral data. Narrow waveband data has a much greater potential for discriminating the features of sensed objects (Lillesand et al. 2008) and hyperspectral imaging is considered to have a greater potential for precise identification, discrimination and classification of studied objects and their features (Treitz and Howarth 1999, Im and Jensen 2008).

Utilization of data acquired using hyperspectral imaging requires specific methodological approaches. There are two groups of methods used for hyperspectral data analyses: methods for reducing the data dimension and methods for information extraction (Hi et al. 1998, Mitra and Murthy 2002, Bajcsy and Groves 2004). As hyperspectral cubes contain hundreds of contiguous spectral bands, the neighbouring wavebands have a high degree of correlation, which results in information redundancy through oversampling (Thenkabail et al. 2004). Thus, the most informative spectral bands need to be selected for further processing. For hyperspectral images acquired under laboratory conditions, widely used methods for data dimension reduction are dispersion analysis (Manevski et al. 2011), estimation of coefficients of correlation (Thenkabail et al. 2000, Gomez-Chova et al. 2004, Bajwa et al. 2009) and principal component analysis (De Backer et al. 2005, Kalacska et al. 2007, Torbick and Becker 2009, Song et al. 2011, Hesketh and Sįnchez-Azofeifa 2012, Koonsanit et al. 2012).

The most commonly used methods for information extraction from hyperspectral data are modelling and classification (Du and Chang 2000, Gong et al. 2003, Camps-Valis and Bruzzone 2005, Bajwa and Vories 2007). Modelling is used, when the characteristics needed for quantification are numerical. A model of a mathematical relationship is developed based on, for example, an estimation of chlorophyll, nitrogen and/or other concentrations of chemical elements in the foliage of trees (Gong et al. 1995, Gastellu-Etchegorry et al. 1995, Bajwa and Vories 2007). Classification is used, when the characteristics of interest are categorical, e.g. if dealing with the recognition of different forest tree species or land-cover types (Du and Chang 2000, Camps-Valis and Bruzzone 2005). The most widely used modelling methods are multivariate regression (Gong et al. 1995, Gastellu-Etchegorry et al. 1995, Bajwa and Vories 2007) and partial least squares regression (Wold et al. 2001, Smith et al. 2002, McDonald et al. 2003, Bajwa 2006, Cho et al. 2007, Asner and Martin 2008, Bajwa et al. 2009, Carrascal et al. 2009). A very widely used method for classification is discriminant analysis (Gong et al. 1997, Fung et al. 1998, Du and Chang 2000, Camps-Valis and Bruzzone 2005, Clark et al. 2005).

The aim of our study was to evaluate the potential of laboratory acquired hyperspectral image data to assess various chemical properties of Scots pine needles and the crown defoliation status of the tree the needles were collected from. We aimed to integrate

particular methodical solutions that assess the diverse characteristics of Scots Pine needles that could be used to describe the overall condition of a tree. Scots pine is one of the most common and commercially important tree species in Lithuania. According to the State Forest Service (2012), Scots pine stands make up 35.1% of the total forest area in Lithuania, is considered to be a good indicator of environmental conditions and has become the focus of many forest health related studies (Solberg et al. 2006, Augustaitis et al. 2007, Juknys et al. 2013).

The objectives of this study included the following:

1. Investigating whether it was possible to determine the defoliation of Scots Pine crowns using hyperspectral imaging under laboratory conditions and to select the wavebands which best represented the spectral differences between various crown defoliation classes.

2. Examining the relationships between the hyperspectral reflectance properties of Scots pine needles and the concentrations of their chemical constituents using hyperspectral imaging under laboratory conditions.

## Materials and Methods

A total of 67 mature Scots pine trees, with crown defoliation ranging from 0% to 80%, were selected for foliage spectral sampling. The crown defoliation was visually assessed in the forest by two experienced specialists from the Forest Monitoring Laboratory of 'Aleksandras Stulginskis' University according to the methods and criteria for harmonized sampling, assessment, monitoring and analysis of the effects of air pollution on forests (Eichhorn et al. 2010). Defoliation assessment is conducted annually, as part of a long term monitoring programme; in permanent plots located in mature Scots pine stands found at the Aukštaitija integrated monitoring station. The trees sampled were located in two forest compartments: a) a pure Scots pine stand, age: 103 years, mean height: 29 m, mean diameter (at 1.3 m height): 35 cm, standing volume: 313 $m^3$/ha, site type: *Vaccinio myrtillosa* and plot coordinates according to WGS 1984 coordinate system: E25.982, N55.483 and b) a pure Scots pine stand, age: 178 years, mean height: 31 m, mean diameter (at 1.3 m height): 40 cm, standing volume: 463 $m^3$/ha, site type: *Vaccinio myrtillosa* and plot coordinates according to WGS 1984 coordinate system: E26.060, N55.449.

Climbing equipment and a telescopic cutter were used to collect the needle samples. One sample branch from the western, northern and eastern sides and four sample branches from the southern side of the middle-upper part of the crown of each tree were cut making seven branches per tree in total. To consider the influence of the needles age, current and previous year sprouts were collected. The samples were taken between July 29 and August 10, 2012. The needles from the branches, which receive maximal solar radiation, i.e. the ones collected from the southern side of crowns were also used for chemical analyses (totally 240 branches). The cut samples were immediately packed into plastic bags. The bags were labelled, put into portable cooler bags and transported to the laboratory for immediate spectral measurements, which were completed within 14 hours of cutting the first sample. Separate equivalent sub-samples were made for needles from the current and previous year sprouts by harvesting every needle from the sprouts.

Analyses of needle chemical constituents were performed at the Agrochemical Research Laboratory of the Lithuanian Research Centre for Agriculture and Forestry. Concentrations of nitrogen, phosphorus, calcium, magnesium, potassium, iron, copper, manganese, zinc and boron were measured. The element concentrations in the needles were measured according to the requirements of following EEC directives: nitrogen: 72/199/EEB, phosphorus: 71/393/EEB, calcium: 71/250/EEB, magnesium: 73/46/EEB and potassium: 71/250/EEB. The concentrations of iron, copper, manganese, zinc and boron were measured according to the requirements of Lithuanian standard LST CEN/TS 15621:2007.

The prepared samples were scanned using a hyperspectral camera VNIR400H. This device was equipped with a highly sensitive VNIR spectrometer capable of covering the 400-1,000 nm spectral range with a sampling interval of 0.6 nm and produced 955 spectral bands. The spatial data from each scanned sample was recorded in a charged-coupled device (CCD) array with a 1,392 × 1,000 pixel resolution (pixel size was 6.45 μm × 6.45 μm). The camera, using a field of view of 30 degrees, was mounted on a copy stand and was oriented in the nadir position with the lens fixed at 33 cm above the sample. Two 100 W halogen lamps, which can provide stable electro-magnetic radiation in the 400-1,000 nm range, were used for sample illumination. The halogen lamps were fixed symmetrically on both sides of the camera lens and illuminated the sample by allowing their light beams to criss-cross above the sample. The scanning room was darkened to avoid unrelated spectral signals from ambient light sources.

The needles were spread on top of a matt black painted plate so that the background plate was fully covered by needles. The spectral response of each needle sample was recorded four times. The background plate was rotated 90 degrees horizontally af-

ter every hyperspectral sample to correct for the bidirectional reflectance distribution. These steps were repeated for all samples. The results were raw hyperspectral images of the needle samples (four for each separate sample).

Next, the radiance curve was converted to a reflectance curve for each image pixel. Completed target measurements were compared against measurements taken from a reference panel of known spectral reflectances (Avian Technologies LLC 99% white reference panel). The spectrometer internal current (dark current) was also corrected. The resulting spectra were then smoothed using the Savitzky-Golay filter function with a 4th-order polynomial fit and 25 data points. The steps above were repeated for each hyperspectral image. Aiming to have a fixed number of pixels in a standard dimension grid and each pixel containing only spectral signals related to the needles spectral reflectance, the images were then cropped to 400 × 400 pixels in size by spatially subsetting the hyperspectral images. The mean spectra of latter images were calculated.

Thus, four reflectance curves were derived from the four needle sample images and then averaged to construct a single reflectance curve for each sample. A total of 938 reflectance curves were constructed. Each reflectance curve was treated as a series of numbers (reflectance coefficients) and was used for statistical analyses. The sizes of samples used in analyses are presented in Table 1.

The distribution of the spectral responses at every spectral band was tested for normality using the Shapiro-Wilk test ($\alpha = 0.05$) and the homogeneity of the variance was checked using Levene's test ($\alpha = 0.05$). Only the homoscedastic and normally distributed ($p > \alpha$) spectral data for every spectral band were used in further analyses.

Principal component analysis (PCA) was employed to reduce the dimensionality and redundancy inherent in hyperspectral data. PCA reduces the data to a set of orthogonal eigenvectors, which maximize variation and greatly reduce autocorrelation (Wold 1966). The nonlinear iterative partial least squares (NIPALS) algorithm was employed in the calculations (Wold 1966, Wold et al. 1987). In this study, principal component analysis was used to compute the contribution of the reflectance coming from each wavelength to the principal components. Wavebands were treated as independent variables. The reflectance data from all the samples were analysed. The data were pre-processed using unit variance scaling and mean-centering procedures. Component loadings were computed for each latent variable waveband (principal components (PCs) or factors). Component loadings represented the relative degree, to which each variable (waveband) explained the relationship between the component and sampled tree species. If the component covered a significant portion of the overall data variance that is related to the differentiation of samples, then the wavebands with the highest loadings on that component were better suited for defoliation differentiation. Therefore the wavebands with the highest absolute values for component loadings were selected as most suitable ones for optimally discriminating various levels of crown defoliation. The aim was to select as many PCs that, together, explained 99% or more of the variance.

The subject-related information was extracted after selecting the most informative wavebands. The relationship between Scots pine crown defoliation and needle spectral reflectance properties was assessed by evaluating the potential to determine the particular defoliation class. The foliage samples were classified into defoliation classes by employing linear discriminant analysis and by using reflectance values from the most informative wavebands as discriminating variables. The samples were classified into the following classes:

1. Nine defoliation classes at 5% interval, i.e. the classes that are used after visual assessment of the forest.

2. Four defoliation classes, based on the UNECE definition (none: up to 10%; slight: >10–25%, moderate: >25–60% and severe: over 60%).

3. Three defoliation classes (up to 30%, > 30–50% and over 50%).

**Table 1.** Sample sizes

| Number of trees selected for the study | Number of sample branches per tree | Total number of sample branches | Total number of the needle samples (separated needles of current and previous years) | Samples which data passed the normality tests and were used: | | | | | |
|---|---|---|---|---|---|---|---|---|---|
| | | | | for PCA and LDA | | for building of PLSR models | | for validation of PLSR models | |
| | | | | Current year needle | Previous year needle | Current year needle | Previous year needle | Current year needle | Previous year needle |
| 67 | 7 | 469 | 938 | 469 | 420 | 240 | 240 | 80 | 80 |

The overall classification accuracy was estimated by calculating the proportion of correctly classified needle samples, compared to the total number of classified samples. Producer's accuracy, User's accuracy and kappa statistics were also calculated. The Z statistic was calculated to check whether the error matrix kappa statistics for the different classifications were significantly different, i.e. to check whether the classification accuracy increased/decreased significantly (Congalton and Green 1999).

Partial least squares regression (PLSR) analysis was used to predict the concentrations of chemical constituents in needles. PLSR is well suited to analysing a large array of related predictor variables (i.e. not truly independent), where the sample size that is not large enough, when compared to the number of independent variables (Wold et al. 2001, Carrascal et al. 2009).

The concentrations of nitrogen, phosphorus, calcium, magnesium, potassium, iron, copper, manganese, zinc and boron in Scots pine needle samples from current and previous years were predicted using needle spectral reflectance data by building partial least squares regression (PLSR) models. PLSR models were built independently for each chemical constituent. The values of one attribute (concentration) of the data set were used to represent the dependent variable and the wavelength reflectance values of the needle samples represented the predictors. The data were pre-processed using unit variance scaling and mean-centering procedures. The detected outliers were deducted from further calculations. The cross-validated determination coefficient ($R^2$) and correlation coefficient ($R$) were calculated for each model. Models were also validated using external data sets that were created by randomly selecting 30% of the samples from the initial data sets. The root mean square errors of prediction (RMSEP) and mean absolute percentage errors (MAPE) were estimated. For the best predicted chemical constituents (MAPE not exceeding 11 % in case of previous and current year), the wavebands most tightly related to their concentration in the needles, were identified. In this study, regression coefficients resulting from the PLSR models were used for identifying the most sensitive wavelengths. The central wavebands situated on the three highest peaks of curves formed from absolute values of regression coefficients were found to be the most sensitive ones.

The relationships between crown defoliation and the chemical constituents of their needles were also assessed by linear discriminant analysis, which classified needle samples into three defoliation classes (up to 30%, >30–50% and over 50%) and used the chemical constituent concentrations as discriminating variables.

## Results

The spectral reflectance properties of needles from Scots pine crowns showing various levels of defoliation are summarized in Figure 1. The spectral reflectance curves of the needles from crowns with higher levels of defoliation feature a higher reflectance in the green–red (495–680 nm) spectral zone and a lower reflectance in the near infrared (750–1,000 nm) zone. This is particularly evident in spectral curves that have been generalized to present defoliation classes 3 and 4 (Figure 1 b, c, e and f).

PCA revealed, that more than 99% of total spectral reflectance data variance in current (2012) and previous (2011) year needles was explained by five and six PCs respectively (Table 2). Thus, the five wavebands for the current year needles and the six wavebands for the previous year needles were selected as the optimal ones for discriminating the defoliation classes. The wavelengths of the optimal bands varied for current and previous year needles but their position in the spectral interval was contiguous.

The ability to spectrally discriminate the needle samples of differently defoliated Scots pine crowns was

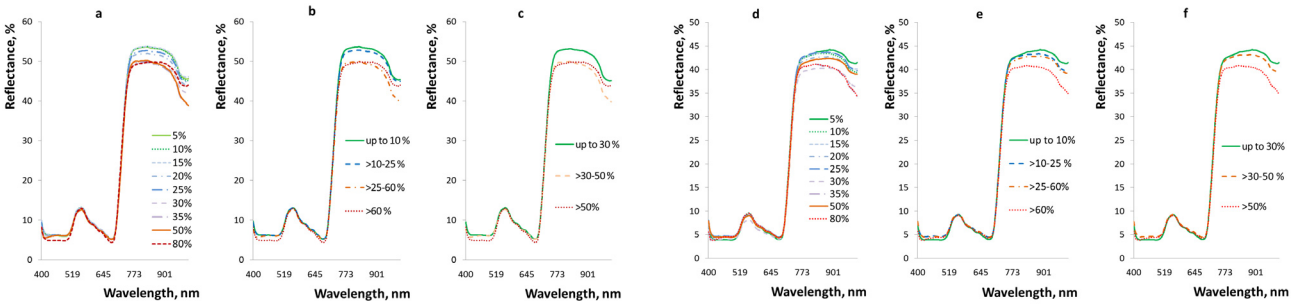


**Figure 1.** Generalized spectral curves for Scots pine needles: a) nine defoliation classes, current year needles, b) four defoliation classes, current year needles, c) three defoliation classes, current year needles, d) nine defoliation classes, previous year needles, e) 4 defoliation classes, previous year needles, f) 3 defoliation classes, previous year needles

**Table 2.** Variance explained by the principal components and the wavelengths most sensitive to Scots Pine crown defoliation

| Needle age | Principal component (PC) | | | | | | | | | | | |
|---|---|---|---|---|---|---|---|---|---|---|---|---|
| | PC1 | | PC2 | | PC3 | | PC4 | | PC5 | | PC6 | |
| | Variance explained | Most informative wavelength | Variance explained | Most informative wavelength | Variance explained | Most informative wavelength | Variance explained | Most informative wavelength | Variance explained | Most informative wavelength | Variance explained | Most informative wavelength |
| Current year (2012) | 60.5% | 735.4 nm | 27.7% | 969.3 nm | 6.2% | 713.1 nm | 3.5% | 683.1 nm | 1.6% | 406.9 nm | - | - |
| Previous year (2011) | 52.2% | 737.4 nm | 28.2% | 968.7 nm | 9.4% | 419.9 nm | 6.4% | 680.6 nm | 2.8% | 400.1 nm | 0.5% | 688.2 nm |

assessed by examining the classification accuracy using linear discriminant analysis. The reflectance values of the optimal wavebands were used as discriminating variables. Samples representing different needle ages were classified separately. Classification results are summarized in Tables 3–4. The accuracy of classification into three defoliation classes is not reported in the tables as all samples are correctly classified, yielding a 100% overall classification accuracy.

The results revealed that it was not possible to precisely determine nine defoliation classes for Scots pine crowns (i.e. the ones employed when the trees are visually assessed according to the methods used by forest health monitoring surveys) according to

**Table 3.** The classification accuracy of Scots pine needle samples (psc.) into nine defoliation classes

| **Visually assessed defoliation, %** | **Predicted defoliation, %** | | | | | | | | | Total | **"Producer's" accuracy, %** |
|---|---|---|---|---|---|---|---|---|---|---|---|
| | 5 | 10 | 15 | 20 | 25 | 30 | 35 | 50 | 80 | | |
| **Current year needles** | | | | | | | | | | | |
| 5 | 0 | 7 | 21 | 7 | 14 | 0 | 0 | 0 | 0 | 49 | **0.0** |
| 10 | 0 | 0 | 42 | 14 | 7 | 14 | 0 | 0 | 0 | 77 | **0.0** |
| 15 | 14 | 0 | 77 | 14 | 0 | 7 | 0 | 0 | 0 | 112 | **68.8** |
| 20 | 0 | 7 | 21 | 21 | 0 | 14 | 0 | 0 | 0 | 63 | **33.3** |
| 25 | 0 | 14 | 28 | 7 | 0 | 14 | 0 | 0 | 0 | 63 | **0.0** |
| 30 | 0 | 0 | 21 | 0 | 0 | 42 | 0 | 0 | 0 | 63 | **66.7** |
| 35 | 0 | 0 | 0 | 0 | 0 | 0 | 14 | 0 | 0 | 14 | **100.0** |
| 50 | 0 | 0 | 0 | 0 | 0 | 0 | 0 | 14 | 0 | 14 | **100.0** |
| 80 | 0 | 0 | 0 | 0 | 0 | 0 | 0 | 0 | 14 | 14 | **100.0** |
| Total | 14 | 28 | 210 | 63 | 21 | 91 | 14 | 14 | 14 | 469 | |
| **"User's" accuracy, %** | **0.0** | **0.0** | **36.7** | **33.3** | **0.0** | **46.2** | **100.0** | **100.0** | **100.0** | | |
| **Kappa statistic** | | | **0.26** | **Overall classification accuracy, %** | | | | | | | **38.8** |
| **Previous year needles** | | | | | | | | | | | |
| 5 | 7 | 14 | 21 | 0 | 7 | 0 | 0 | 0 | 0 | 49 | **14.3** |
| 10 | 7 | 14 | 14 | 28 | 7 | 0 | 0 | 0 | 0 | 70 | **20.0** |
| 15 | 14 | 7 | 56 | 14 | 0 | 0 | 0 | 0 | 0 | 91 | **61.5** |
| 20 | 7 | 7 | 35 | 21 | 0 | 0 | 0 | 0 | 0 | 70 | **30.0** |
| 25 | 7 | 0 | 21 | 21 | 14 | 0 | 0 | 0 | 0 | 63 | **22.2** |
| 30 | 7 | 0 | 0 | 7 | 0 | 21 | 0 | 0 | 0 | 35 | **60.0** |
| 35 | 0 | 0 | 0 | 0 | 0 | 0 | 7 | 7 | 0 | 14 | **50.0** |
| 50 | 0 | 0 | 0 | 0 | 0 | 0 | 0 | 14 | 0 | 14 | **100.0** |
| 80 | 0 | 0 | 0 | 0 | 0 | 0 | 0 | 0 | 14 | 14 | **100.0** |
| Total | 49 | 42 | 147 | 91 | 28 | 21 | 7 | 21 | 14 | 420 | |
| **"User's" accuracy, %** | **14.3** | **33.3** | **38.1** | **23.1** | **50.0** | **100.0** | **100.0** | **66.7** | **100.0** | | |
| **Kappa statistic** | | | **0.29** | **Overall classification accuracy, %** | | | | | | | **40.0** |

**Table 4.** The classification accuracy of Scots pine needle samples (psc.) into four defoliation classes

| **Visually assessed defoliation, %** | **Predicted defoliation, %** | | | | Total | **"Producer's" accuracy, %** |
|---|---|---|---|---|---|---|
| | up to10 | >10-25 | >25-60 | >60 | | |
| **Current year needles** | | | | | | |
| up to10 | 0 | 112 | 14 | 0 | 126 | **0.0** |
| >10-25 | 0 | 217 | 21 | 0 | 238 | **91.2** |
| >25-60 | 0 | 28 | 63 | 0 | 91 | **69.2** |
| >60 | 0 | 0 | 0 | 14 | 14 | **100.0** |
| Total | 0 | 357 | 98 | 14 | 469 | |
| **"User's" accuracy, %** | **0.0** | **60.8** | **64.3** | **100.0** | | |
| **Kappa statistic** | **0.35** | **Overall classification accuracy, %** | | | | **62.7** |
| **Previous year needles** | | | | | | |
| up to 10 | 28 | 91 | 0 | 0 | 119 | **23.5** |
| >10-25 | 14 | 203 | 7 | 0 | 224 | **90.6** |
| >25-60 | 0 | 7 | 56 | 0 | 63 | **88.9** |
| >60 | 0 | 0 | 0 | 14 | 14 | **100.0** |
| Total | 42 | 301 | 63 | 14 | 420 | |
| **"User's" accuracy, %** | **66.7** | **67.4** | **88.9** | **100.0** | | |
| **Kappa statistic** | **0.50** | **Overall classification accuracy, %** | | | | **71.7** |

needle hyperspectral reflectance data. The overall classification accuracy did not exceed 40% when classifying current and previous year needles and the kappa statistic values were only at the 'fair' level of 0.26 and 0.29, respectively (Table 3). The needle samples taken from crowns with none (up to 10%) and slight (> 10–25%) defoliation had very similar spectral reflectances, which caused low classification accuracy, especially for current year needles. User's accuracy for current year needles ranged from 0% to 36.7% and from 14.3% to 50.0% for previous year needles, i.e. the needle samples were consistently misclassified into the wrong defoliation classes. The classification accuracy of needle samples taken from the moderately (>30–50%) and severely (> 60%) defoliated crowns revealed that spectral differences tended to increase according to their level of defoliation. Current year needle samples taken from crowns with 35% defoliation or higher were correctly classified into their respective classes.

Combining the samples into groups according to the UNECE definition (none: up to 10%; slight: > 10–25%, moderate: > 25–60% and severe: over 60%) raised the overall classification accuracy to up to 62.7% for current year needles and up to 71.7% for previous year needles (Table 4). The kappa statistic didn't improve significantly ($Z$ = 1.78) for the current year needles (kappa = 0.35) but it did ($Z$ = 4.23) for the previous year needles (kappa = 0.50) (Table 4). The very similar spectral reflectance properties of the needle samples taken from crowns with none (up to 10%) and slight (> 10–25%) defoliation were the reason for relatively low classification accuracy in this case too. The overall classification accuracy increased significantly and reached 100%, after grouping the samples into three groups (up to 30%, >30–50% and over 50%).

The nitrogen, phosphorus, calcium, magnesium, potassium, iron, copper, manganese, zinc and boron concentrations in Scots pine current (2012) and previous (2011) year needles are presented in Table 5.

Needle age had a significant effect on the concentrations of all the measured elements (Table 6). The concentration of nitrogen in the previous year needles of Scots pine was 4% higher, compared to the current year needles, the concentration of manganese was 53% higher and copper was 76% higher. Thus needle age has to be considered when estimating the concentration of the chemical constituents in needles.

The needle samples were classified into three defoliation classes (up to 30%, > 30–50% and over 50%) using the chemical constituent concentrations as discriminating variables. Good and not significantly different ($Z$ = 0.48) classification accuracies (kappa = 0.83 for current year needles and kappa = 0.90 for previous year needles) were achieved. Thus the concentrations of needle chemical constituents were found to be related to Scots pine crown defoliation when relatively large defoliation differences were investigated.

The accuracies for chemical constituent predictions in Scots pine needles using their hyperspectral reflectance data as discriminating variables and the PLSR are summarized in Table 7. The prediction accuracy for needle chemical constituent concentrations was dependent on needle age. For current year needles, a moderate positive linear relationship between actual and predicted concentrations values was determined for nitrogen ($R$ = 0.61), phosphorus and zinc ($R$ = 0.57), calcium ($R$ = 0.56), manganese ($R$ = 0.49) and

**Table 5.** Concentrations of the measured elements in Scots Pine needle samples

| Element | Number of samples | Current year needles | | | | Previous year needles | | | |
|---|---|---|---|---|---|---|---|---|---|
| | | Average | Standard deviation | Minimum | Maximum | Average | Standard deviation | Minimum | Maximum |
| Nitrogen, % | 60 | 1.18 | 0.09 | 0.99 | 1.38 | 1.23 | 0.11 | 1.01 | 1.44 |
| Phosphorus, % | 60 | 0.13 | 0.02 | 0.09 | 0.16 | 0.10 | 0.01 | 0.08 | 0.13 |
| Potassium, % | 60 | 0.48 | 0.06 | 0.36 | 0.64 | 0.34 | 0.05 | 0.23 | 0.49 |
| Calcium, % | 60 | 0.18 | 0.03 | 0.13 | 0.27 | 0.39 | 0.08 | 0.21 | 0.65 |
| Magnesium, % | 60 | 0.10 | 0.01 | 0.07 | 0.15 | 0.07 | 0.01 | 0.04 | 0.11 |
| Iron, mg/kg | 60 | 52.64 | 63.44 | 24.50 | 542.00 | 73.38 | 28.96 | 45.10 | 186.00 |
| Copper, mg/kg | 60 | 5.18 | 1.50 | 3.00 | 11.00 | 3.31 | 1.75 | 1.80 | 12.60 |
| Manganese, mg/kg | 60 | 434.40 | 120.60 | 189.00 | 758.00 | 935.74 | 251.49 | 500.00 | 1589.00 |
| Zinc, mg/kg | 60 | 35.97 | 8.69 | 20.10 | 58.90 | 43.51 | 10.87 | 21.10 | 74.30 |
| Boron, mg/kg | 60 | 14.28 | 3.27 | 8.55 | 22.50 | 12.09 | 3.64 | 4.70 | 21.50 |

**Table 6.** The difference in element concentrations between previous year needles and current year needles

| Element | Nitrogen | Phosphorus | Potassium | Calcium | Magnesium | Iron | Copper | Manganese | Zinc | Boron |
|---|---|---|---|---|---|---|---|---|---|---|
| The difference in element concentrations between previous year needles and current year needles | 4.1 | -27.5 | -41.8 | 52.0 | -45.3 | 21.1 | -75.9 | 53.1 | 13.8 | -24.7 |
| Significance of difference (*p-value*) | 0.001 | $1.19 \times 10^{-21}$ | $2.89 \times 10^{-27}$ | $2.31 \times 10^{-41}$ | $2.26 \times 10^{-24}$ | 0.015 | $5.27 \times 10^{-10}$ | $4.63 \times 10^{-30}$ | $1.67 \times 10^{-05}$ | 0.0003 |

**Table 7.** Model validation statistics illustrating the prediction accuracy of the PLSR models used to predict the content of chemical constituents in needles employing hyperspectral reflectance as predictors and chemical contents as response variables (numerator refers to the current year, denominator refers to the previous year needles)

| Statistics \ Element | Boron | Calcium | Copper | Iron | Potassium | Magnesium | Manganese | Nitrogen | Phosphorus | Zinc |
|---|---|---|---|---|---|---|---|---|---|---|
| *R* | 0.33<br>0.60 | 0.56<br>0.35 | 0.20<br>0.04 | 0.26<br>0.21 | 0.40<br>0.33 | 0.20<br>0.10 | 0.49<br>0.31 | 0.61<br>0.46 | 0.57<br>0.49 | 0.57<br>0.13 |
| $R^2$ | 0.11<br>0.36 | 0.31<br>0.12 | 0.04<br>0.00 | 0.07<br>0.04 | 0.16<br>0.11 | 0.04<br>0.01 | 0.24<br>0.10 | 0.37<br>0.21 | 0.32<br>0.24 | 0.33<br>0.02 |
| *RMSEP* | 3.36<br>2.85 | 0.03<br>0.07 | 1.08<br>0.66 | 20.19<br>14.03 | 0.05<br>0.05 | 0.01<br>0.02 | 91.90<br>245.30 | 0.08<br>0.09 | 0.02<br>0.01 | 6.66<br>11.19 |
| *MAPE* | 18.1<br>17.8 | 12.3<br>14.6 | 19.7<br>16.6 | 27.0<br>16.1 | 9.6<br>10.6 | 9.9<br>18.2 | 14.2<br>22.3 | 6.1<br>5.8 | 10.9<br>6.3 | 16.2<br>20.5 |

potassium ($R$ = 0.4). MAPEs of less than 10% were obtained for nitrogen (6.1%) and potassium (9.1%) concentrations. The actual and predicted concentrations for boron, copper, iron and magnesium had low positive linear relationships (0.2 d≤$R$ d≤0.33). In the previous year needles, positive linear relationships between actual and predicted concentrations were determined only for boron ($R$ = 0.6), phosphorus ($R$ = 0.49) and nitrogen ($R$ = 0.46). For current year needles, MAPEs of less than 10% were obtained for predicted concentrations of nitrogen (5.8%) and phosphorus (6.3%). The relationship between actual and predicted concentrations for other constituents was low (0.2 d≤$R$ d≤0.33) for calcium, potassium, manganese and iron or very low (0.01 d≤$R$ d≤0.19 ) for copper, magnesium, and zinc.

These results show that the hyperspectral reflectance of Scots pine needles can be used to predict the concentrations of some chemical constituents in needles. The prediction accuracy was not related to the concentration of a particular element. The best prediction accuracy was obtained for nitrogen (MAPE = 6.1% for current year and 5.8% for previous year needles), phosphorus (MAPE = 10.9% for current year and 6.3% for previous year needles) and potassium (MAPE = 9.6% for current year and 10.6% for previous year needles) concentrations. The wavebands most tightly related to the concentrations of latter chemical constituents are presented in Table 8. No reliable prediction results were obtained for copper, iron and magnesium concentrations.

## Discussion and Conclusions

The results of our study revealed that the majority (~ 60%) of the optimal wavebands for Scots Pine crown defoliation determination were located in the red edge (680 nm–750 nm). This complements the findings of other studies and proves that the red edge reveals the most about tree stress. For example, Luther and Carroll (1999) found that foliage reflectance at 711 nm was the most sensitive to tree stress while investigating various levels of growth vigour in Balsam fir (*Abies balsamea* (L.) Mill.). Carter and Knapp (2001) discovered that an increase in reflectance at 709–718 nm was the most sensitive to plant stress, when they investigated the effects of various stressors on the foliage reflectance by various species, including loblolly pine (*Pinus taeda* L.), radiate pine (*Pinus radiata* D. Don) and longleaf pine (*Pinus palustris* Miller). Eitel et al. (2010) analyzed stress-induced changes in the concentration of chlorophyll in nursery-grown Scots pine seedlings and found that the accuracy of the estimates improved after measuring seedlings reflectance at 730 nm.

The majority of studies using hyperspectral imaging that had focused on the remote assessment of crown defoliation in forest stands were based on the use of remote sensing platforms as the carriers of hyperspectral sensors. Working with airborne sensor-acquired hyperspectral imagery has the advantage of being able to utilize both the spatial and spectral in-

**Table 8.** The most sensitive wavelengths selected according to PLS regression coefficients

| Chemical constituent | Previous year (2011) needles | Current year (2012) needles |
|---|---|---|
| | Central wavebands, nm | |
| Nitrogen | 554.1; 678.6; 711.8 | 405.7; 559.0; 715.7 |
| Phosphorus | 403.5; 687.6; 841.2 | 403.5; 554.1; 718.2 |
| Potassium | 446.8; 570.2; 708.0 | 464.5; 644.7; 750.8 |

formation from the hyperspectral image. Incorporating the hyperspectral image spatial factor usually increases the prediction accuracies, as was shown by Moskal and Franklin (2004). The full potential of airborne hyperspectral images was employed on pure aspen stands to predict their defoliation. A very good regression model ($R^2$ = 0.93) fit was achieved when spectral and spatial data were used. When the spatial data were eliminated from the regression model, the prediction potential decreased substantially ($R^2$ = 0.54). Thus, the remotely captured hyperspectral images are a product of spectral reflectance properties that are significantly affected by numerous factors, such as: the structure of the objects being sensed and the radiation transfer properties through the atmosphere (Asner 1998, Roberts et al. 2004). Getting the hyperspectral images from shorter distances usually increases the potential for hyperspectral imaging to detect the properties inherent to the objects being studied, especially the chemistry of tree foliage (Kokally and Clark 1999, Asner and Martin 2008). Thus, the hyperspectral imagery investigations under laboratory conditions could be considered an accurate method as it can potentially deal with physical and chemical properties of the objects under investigation.

In our study, using pure needle spectral reflectance data as predictors enabled us to precisely classify Scots pine needles into three defoliation classes. A very good classification precision of needles into the same three defoliation classes was also achieved using only needle chemistry data as predictors. This proved that the pure needle reflectance spectra have strong relationship with needle chemical constituents.

However, the success at predicting concentrations of chemical constituents in Scots pine needles by their hyperspectral reflectance data was variable. The concentrations of nitrogen, phosphorus, zinc, calcium, boron and potassium could be predicted using Scots pine needle hyperspectral reflectance data obtained under laboratory conditions, although only moderate prediction accuracies were achieved. Concentrations of copper, iron, and magnium were not found to have a relationship with pine needle hyperspectral reflectance spectra.

In our study, the foliage of only one species (Scots pine) was used to investigate the relationships between the spectral reflectance of needles and their chemical constituents. This prevented the prediction accuracy being influenced by spectral reflectance differences due to different species, but it may explain why the prediction accuracies achieved in our study were relatively low compared to the results of similar studies by other authors. For example, a study conducted by Ferwerda and Skidmore (2007) showed prediction successes for phosphorus, potassium, calcium, magnesium and sodium concentrations when three tree species, willow (*Salix cinera* L.), mopane (*Cholophospermum mopane*) and olive (*Olea europaea* L), and one shrub species, heather (*Calluna vulgaris* L), were investigated together. The relationships between the concentrations of chemical constituents and foliage spectral reflectance data may possibly have been improved by the differences in the foliage chemical constituents between the species, which could have been caused by the covariance with other properties of individual species. This was shown in the study by Axelsson et al. (2013), in which concentrations of nitrogen, phosphorus, potassium, calcium, magnesium and sodium in the foliage of various Indonesian mangrove species were investigated. Prediction accuracies for phosphorus, potassium, calcium, sodium and magnesium were strongly influenced by one mangrove species that had much lower concentrations of these elements.

Two primary conclusions are drawn from this study:

1. The hyperspectral reflectance data allowed us to reliably (100% overall classification accuracy) classify the samples into the following defoliation classes: up to 30%, >30–50% and over 50%. However, the Scots pine needle samples were not accurately classified using hyperspectral data acquired under laboratory conditions into the nine defoliation classes used, when the trees are visually assessed in the forest.

2. Concentrations of nitrogen ($R$ = 0.61, MAPE = 6%), boron ($R$ = 0.6, MAPE = 18%), phosphorus ($R$ = 0.57, MAPE = 11%), zinc ($R$ = 0.57, MAPE = 16%), calcium (R = 0.56, MAPE = 12%), manganese (R = 0.49, MAPE = 14%) and potassium (R = 0.4, MAPE = 10%) could be predicted using Scots pine needle hyperspectral reflectance data obtained under laboratory conditions. The concentrations of the elements in current and previous year needles were significantly different. The concentrations of nitrogen, phosphorus, zinc, calcium and potassium were more successfully predicted using the hyperspectral reflectance data from the current year, whereas the concentration of boron was more successfully predicted using the previous year data.

## Acknowledgements

*This study was carried out within the framework of the national project No VP1-3.1-ŠMM-08-K-01-025 entitled "Specific, genetic diversity and sustainable development of Scots pine forest to mitigate the negative effects of increased human pressure and climate change" supported by the European Social Fund. The manuscript is also supported by Life Environment Project LIFE08 ENV/IT/000339.*

## References

**Ardö, J.** 1998. Remote Sensing of Forest Decline in the Czech Republic. Lund University, Department of Physical Geography, Sweden. 47 pp.

**Asner, G.P.** 1998. Biophysical and biochemical sources of variability in canopy reflectance. *Remote Sensing of Environment* 64: 234-253.

**Asner, G. P. and Martin, R. E.** 2008. Spectral and chemical analysis of tropical forests: scaling from leaf to canopy levels. *Remote Sensing of Environment* 112 (10): 3958-3970.

**Augustaitis, A., Augustaitienė, I. and Deltuvas, R.** 2007. Scots pine (*Pinus sylvestris* L.) crown defoliation in relation to the acid deposition and meteorology in Lithuania. *Water, Air, and Soil Pollution* 182: 335-348.

**Axelsson, C., Skidmore, A. K., Schlerf, M., Fauzi, A. and Verhoef, W.** 2013. Hyperspectral analysis of mangrove foliar chemistry using PLSR and support vector regression. *International Journal of Remote Sensing* 34(5): 1724-1743.

**Bajcsy, P. and Groves, P.** 2004. Methodology for hyperspectral band selection. *Photogrammetric Engineering and Remote Sensing* 70: 793-802.

**Bajwa, S.G.** 2006. Modeling rice plant nitrogen effect on canopy reflectance with partial least square regression. *Transactions of the ASAE* 49: 229-237.

**Bajwa, S.G., Mishra, A.R. and Norman, R.J.** 2009. Canopy reflectance response to plant nitrogen accumulation in rice. *Precision Agriculture* 11: 488-506.

**Bajwa, S.G. and Vories, E.D.** 2007. Spatial analysis of cotton (*Gossypium hirsutum* L.) canopy responses to: irrigation in a moderately humid area. *Irrigation Science* 25: 429-441.

**Camps-Vails, G. and Bruzzone, L.** 2005. Kernel-based methods for hyperspectral image classification. *IEEE Transactions on Geoscience and Remote Sensing* 43: 1351-1362.

**Carrascal, L.M., Galvan, I. and Gordo, O.** 2009. Partial least squares regression as an alternative to current regression methods used in ecology. *Oikos* 118: 681-690.

**Carter, G.A. and Knapp, A.K.** 2001. Leaf optical properties in higher plants: linking spectral characteristics to stress and chlorophyll concentration. *American Journal of Botany* 88: 677–684.

**Cho, M.A., Skidmore, A., Corsi, F., van Wieren, S.E. and Sobhan, L.** 2007. Estimation of green grass/herb biomass from hyperspectral imagery using spectral indices and partial least square regression. *International Journal of Applied Earth Observation and Geoinformation* 9: 414-424.

**Ciesla, W.M.** 2000. Remote Sensing in Forest Health Protection. United States Department of Agriculture, Forest Service, Forest Health Technology Enterprise Team, Remote Sensing Applications Center, FHTET Report No. 00-03. 276 pp.

**Ciesla, W.M., Dull, C.W. and Acciavatti, R.E.** 1989. Interpretation of SPOT-1 color composites for mapping of defoliation of hardwood forests by gypsy moth. *Photogrammetric Engineering and Remote Sensing* 55(10): 1465-1470.

**Clark, M.L., Roberts, D.A. and Clark, D.B.** 2005. Hyperspectral discrimination of tropical rain forest tree species at leaf to crown scales. *Remote Sensing of Environment* 96: 375-398.

**Congalton, R.G. and Green K.** 1999. Assessing the Accuracy of Remotely Sensed Data – Principles and Practices, CRC Press, Boca Raton. 160 pp.

**De Backer, S., Kempeneers, P., Debruyn, W. and Scheunders, P.** 2005. Band selection for hyperspectral remote sensing. *IEEE Geoscience and Remote Sensing Letters* 2: 319-323.

**Du, Q. and Chang, C.I.** 2000. A linear constrained distance-based discriminant analysis for hyperspectral image classification. *Pattern Recognition* 34: 361-373.

**Eichhorn, J., Roskams, P., Ferretti, M., Mues, V., Szepesi, A. and Durrant, D.** 2010. Visual Assessment of Crown Condition and Damaging Agents. Manual Part IV. In: Manual on methods and criteria for harmonized sampling, assessment, monitoring and analysis of the effects of air pollution on forests. UNECE ICP Forests Programme Coordinating Centre, Hamburg, Germany. 49 pp.

**Eismann, M. T.** 2012. Hyperspectral Remote Sensing, SPIE Press, Bellingham, USA. 748 pp.

**Eitel, J. U. H., Keefe, R. F., Long, D.S., Davis, A. S. and Vierling, L.A.** 2010. Active ground optical remote sensing for improved monitoring of seedling stress in nurseries. *Sensors* 10: 2843–2850.

**Ferretti, M.** 1998. Potential and limitation of visual indices of tree condition. *Chemosphere* 4–5: 1031–1036.

**Ferwerda, J. G. and Skidmore, A. K**. 2007. Can nutrient status of four woody plant species be predicted using field spectrometry? *ISPRS Journal of Photogrammetry and Remote Sensing* 62(6): 406-414.

**Fischer, R., Waldner, P., Carnicer, J., Coll, M., Dobbertin, M., Ferretti, M., Hansen, K., Kindermann, G., Lasch-Born, P., Lorenz, M., Marchetto, A., Meining, S., Nieminen, T., Peñuelas, J., Rautio, P., Reyer, C., Roskams, P. and Sánchez, G.** 2012. The Condition of Forests in Europe. 2012 Executive Report. ICP Forests, Hamburg, Germany. 24 pp.

**Fung, T., Ma, F. Y. and Siu, W. L.** 1998. Hyperspectral data analysis for subtropical tree species recognition. In: *Geoscience and Remote Sensing Symposium Proceedings* 3: 1298-1300.

**Gastellu-Etchegorry, J.P., Zagolski, F., Mougtn, E., Marty, G. and Giordano, G.** 1995. An assessment of canopy chemistry with AVIRIS - A case study in the Landes forest, South-west France. *International Journal of Remote Sensing* 16: 487-501.

**Goetz, A.H., Vane, G., Solomon, J.E. and Rock, B.N.** 1985. Imaging Spectrometry for Earth Remote Sensing. *Science* 4704: 1147-1153.

**Gomez-Chova, L., Calpe, J., Camps-Vails, G., Martin, J.D., Soria, E., Vila, J., Alonso-Chorda, L. and Moreno, J.** 2004. Feature selection of hyperspectral data through local correlation and SFFS for crop classification. In: *Proceedings of IEEE International Symposium on Geoscience and Remote Sensing* 1: 555-557.

**Gong, P., Pu, R., Biging, G.S. and Larrieu, M.R.** 2003. Estimation of forest leaf area index using vegetation indices derived from Hyperion hyperspectrai data. *IEEE Transactions on Geoscience and Remote Sensing* 41: 1355-1362.

**Gong, P., Pu, R. and Miller, J.R.** 1995. Coniferous forest leaf area index estimation along the Oregon transect using compact airborne spectrographic imager data. *Photogrammetric Engineering and Remote Sensing* 61: 1107-1117.

**Gong, P., Pu, R. and Yu, B.** 1997. Conifer species recognition: an explanatory analysis of in situ hyperspectral data. *Remote Sensing of Environment* 62: 189–200.

**Heikkilä, J., Nevelainen, S. and Tokola, T.** 2002. Estimating Defoliation in Boreal Coniferous Forests by Combin-

ing Landsat TM, Aerial Photographs and Field Data. *Forest Ecology and Management* 158: 9-23.

**Hesketh, M. and Sánchez-Azofeifa, G.A.** 2012. The effect of seasonal spectral variation on species classification in the Panamanian tropical forest. *Remote Sensing of Environment* 118: 73–82.

**Hi, T.M., Chen, C.H. and Chang, C.L.** 1998. A fast two-stage classification method for high dimensional remote sensing data. *IEEE Transactions on Geosciences and Remote Sensing* 36: 171-181.

**Hildebrandt, G.** 1993. Central European contribution to remote sensing and photogrammetry in forestry. In: Forest resource inventory and monitoring and remote sensing technology: Proceedings of the IUFRO centennial meeting in Berlin, August 31 – September 4, 1992, Japan Society for Forest Planning Press, Faculty of Agriculture, Tokyo University of Agriculture and Technology 3-5-8 Saiwaicho, Fucku, Tokyo, 183 Japan: 196-212.

**Huber, S., Kneubuehler, M., Psomas, A., Itten, K. and Zimmermann, N.** 2008. Estimating foliar biochemistry from hyperspectral data in mixed forest canopy. *Forest Ecology and Management* 256: 491–501.

**Im, J. and Jensen, J.R.** 2008. Hyperspectral remote sensing of vegetation. *Geography Compass* 2: 1943-1961.

**Juknys, R., Augustaitis, A., Venclovienė, J., Kliučius, A., Vitas, A., Bartkevičius, E. and Jurkonis, N.** 2013. Dynamic response of tree growth to changing environmental pollution. *European Journal of Forest Research*: 1-12.

**Kalacska, M., Bohlman, S., Sanchez-Azofeifa, G.A., Castro-Esau, K. and Caelli, T.** 2007 Hyperspectral discrimination of tropical dry forest lianas and trees: Comparative data reduction approaches at the leaf and canopy levels. *Remote Sensing of Environment* 109: 406–415.

**Koonsanit, K., Jaruskulchai, C. and Eiumnoh, A.** 2012. Band selection for dimension reduction in hyperspectral image using integrated information gain and principal components analysis technique. *International Journal of Machine Learning and Computing* 3: p. 248-251.

**Kuhl, W.E.** 1989. A Method to Detect Forest Decline in Germany – Results of a Color-infra-red Airphoto Interpretation. *Forestry* 62: 51-61.

**Lillesand, T.M., Kiefer, R.W. and Chipman, J. W.** 2008. Remote Sensing and Image Interpretation, 6th ed., Wiley, New York, USA, 756 pp.

**Luther, J.E. and Carroll, A.L.** 1999. Development of an Index of Balsam Fir Vigor by Foliar Spectral Reflectance. *Remote Sensing of Environment* 69: 241-252.

**Manevski, K., Manakos, I., Petropoulos, G. P. and Kalaitzidis, Ch.** 2011. Discrimination of common Mediterranean plant species using field spectroradiometry. *International Journal of Applied Earth Observation and Geoinformation* 13: 922–933.

**McDonald, S., Niemann, K.O., Goodenough, D.G., Dyk, A., West, C., Tian H. and Murdoch, M.** 2003. Hyperspectral Remote Sensing of Conifer Chemistry and Moisture. In: *Geoscience and Remote Sensing Symposium IGARSS '03 Proceedings* 1: 552-554.

**Mitra, P., Murthy, C.A. and Pal, S.K.** 2002. Unsupervised feature selection using feature similarity. *IEEL Transactions on Pattern Analysis and Machine Intelligence* 24: 301-312.

**Moorthy, I., Miller, J. and Noland, T.L.** 2008. Estimating chlorophyll concentration in conifer needles with hyperspectral data: An assessment at the needle and canopy level. *Remote Sensing of Environment* 112: 2824–2838.

**Moskal, L. M. and Franklin, S. E.** 2004. Relationship between airborne multispectral image texture and aspen defoliation. *International Journal of Remote Sensing* 25 (14): 2701-2711.

**Ozolinčius, R. and Stakėnas, V.** 1996. Lietuvos miškų būklės monitoringas: 1988–1995 [Monitoring of Lithuanian forests condition: 1988–1995]. Lietuvos miškų institutas, Kaunas, Lithuania (In Lithuanian)

**Ozolinčius, R.** (ed.) 1999. Monitoring of forest ecosystems in Lithuania. Lututė, Kaunas, Lithuania, 308 pp.

**Roberts, D. A., Ustin, S. L., Ogunjemiyo, S., Greenberg, J., Dobrowski, S. Z., Chen, J. and Hinckley, T. M.** 2004. Spectral and structural measures of northwest forest vegetation at leaf to landscape scales. *Ecosystems* 7(5): 545-562.

**Smith, M.L., Ollinger, S.V., Martin, M.E., Aber, J.D., Hallett, R.A. and Goodale, C.L.** 2002. Direct estimation of aboveground forest productivity through hyperspectral remote sensing of canopy nitrogen. *Ecological Applications* 12: 1286-1302.

**Solberg, S., Næsset, E., Lange, H. and Bollandsås, O.M**. 2004. Remote Sensing of Forest Health. International Archieves of Photogrammetry. *Remote Sensing and Spatial Information Sciences* XXXVI – 8/W2: 161-166.

**Solberg, S., Næsset, E., Hanssen, K. H. and Christiansen, E.** 2006. Mapping defoliation during a severe insect attack on Scots pine using airborne laser scanning. *Remote Sensing of Environment* 102(3): 364-376.

**Song, S., Gong, W., Zhu, B. and Huang, X.** 2011. Wavelength selection and spectral discrimination for paddy rice with laboratory measurements of hyperspectral leaf reflectance. *ISPRS Journal of Photogrammetry and Remote Sensing* 66: 672–682.

**Thenkabail, P.S., Enclona, E.A., Ashton, M.S. and Van Der Meer, V.** 2004. Accuracy assessments of hyperspectral waveband performance for vegetation analysis applications. *Remote Sensing of Environment* 91: 354-376.

**Thenkabail, P.S., Smith, R.B. and De-Pauw, E.** 2000. Hyperspectral vegetation indices for determining agricultural crop characteristics. *Remote Sensing of Environment* 71: 158-182.

**Torbick, N. and Becker, B.** 2009. Evaluating Principal Components Analysis for Identifying Optimal Bands Using Wetland Hyperspectral Measurements from the Great Lakes, USA. *Remote Sensing* 1: 408 - 417.

**Treitz, P.M. and Howarth, P.J.** 1999. Hyperspectral remote sensing for estimating biophysical parameters of forest ecosystems. *Progress in Physical Geography* 23: 359-390.

**Wang, Q. and Li, P.** 2012. Hyperspectral indices for estimating leaf biochemical properties in temperate deciduous forests: Comparison of simulated and measured reflectance data sets. *Ecological Indicators* 14: 56–65.

**Wold. H.** 1966. Estimation of principal components and related models by iterative least squares. In Krishnaiah P. R. Multivariate Analysis. Academic Press, New York, USA: 391-420.

**Wold, S., Esbensen, K. and Geladi, P.** 1987. Principal component analysis. *Chemometrics and Intelligent Laboratory Systems* 2: 37–52.

**Wold, S., Sjostrom, M. and Eriksson, L.** 2001. PLS-regression: a basic tool of chemometrics. *Chemometrics and Intelligent Laboratory Systems* 58: 109–130.

**Wulder, M.A., Dymond, C.C., White, J.C., Leckie, D.G. and Carroll, A.L.** 2006. Surveying Mountain Pine Beetle Damage of Forests: a Review of Remote Sensing Opportunities. *Forest Ecology and Management* 221: 27-41.

**Zawila-Niedzwiecki, T.** 1996. The use of GIS and remote sensing for forest monitoring in Poland. Remote Sensing and Computer Technology for Natural Resource Assessment (Saramaki J, Koch B and Lund G, eds). Proceedings of the Subject Group S4.12-00, the University of Joensuu, Faculty of Forestry. *Research Notes* 48: 29-42.

Received 30 December 2013
Accepted 21 October 2014

# ОЦЕНКА ДЕФОЛИАЦИИ КРОН И ХИМИЧЕСКОГО СОСТАВА ХВОИ СОСНЫ ОБЫКНОВЕННОЙ (*PINUS SYLVESTRIS* L.) ПО ДАННЫМ ЛАБОРАТОРНОГО ГИПЕРСПЕКТРАЛЬНОГО СКАНИРОВАНИЯ

**Г. Масайтис, Г. Мозгерис и А. Аугустайтис**

*Резюме*

Методы, основанные на спектрометрировании используя зоны спектрального отражения за пределами чувствительности человеческого зрения, являются наиболее актуальными в области современных исследований оценки санитарного состояния леса. В настоящей работе дефолиация крон и химический состав хвои сосны обыкновенной (*Pinus sylvestris* L.) оценивались на основе данных гиперспектрального сканирования хвои, полученных в лабораторных условиях используя портативную гиперспектральную камеру VNIR 400H, работающую в диапазоне 400-1000 нм. Исследовались образцы хвои 67 деревьев, произрастающих в двух спелых сосновых древостоях в восточной части Литвы, дефолиация крон которых колебалась от 0% до 80% (используя 5% градацию). Для обработки полученных гиперспектральных данных отражения использовался анализ основных компонентов и линейный дискриминантный анализ для классификации образцов хвои по классам дефолиации, а регрессия частичных наименьших квадратов – для прогнозирования концентрации химических компонентов хвои. Установлено, что по данным гиперспектрального отражения определить классы дефолиации, используя пятипроцентную ступень, является затруднительной задачей (каппа статистика составила 0.29 и 0.26 для хвои прошлого и текучего года, соответственно). Однако, группировка образцов по четырём классам дефолиации, в соответствии с рекомендацией UNECE/FAO (дефолиация отсутствует, менее 10%, незначительная: 10-25%; умеренная: 25-60% и сильная: более 60%), существенно улучшило возможности классификации, используя прошлогоднюю хвою (каппа статистика равна 0.50) и несущественно, используя хвою текучего года (каппа статистика 0.35). Группировка на три класса дефолиации (менее 30%, 30-50% и более 50%) была безошибочна (каппа статистики равны 1.0). Установлено, что по данным гиперспектрального отражения в хвое текущего года также можно с умеренной точностью прогнозировать концентрации следующих химических элементов: азота (коэффициент корреляции между фактическим и прогнозированными значениями, оценённый с использованием кросс-проверки, $R$ = 0,61), фосфора ($P$ = 0,57), цинка ($R$ = 0,57), кальция (R = 0,56), марганца ($R$ = 0,49) и калия (0.40), и слабой точностью: бора ($R$ = 0,33), железа ($R$ = 0,26), магния ($R$ = 0,20) и меди ($R$ = 0,20).

**Ключевые слова:** гиперспектральное отражение, гиперспектральные изображения, сосна обыкновенная, дефолиация кроны, химические элементы хвои